Supporting Information for

Confined Entanglement Networks Coordinate Hierarchical Energy Dissipation in Super-Tough Hydrogels

Huijun Zhang[a,b,#], Yingzhang Liu[a,b,#], Jinxian Liu[a,b], Cuilian Qiu[a,b], Yanqun Huang[a,b], Weibing Xue[a,b], Huanxin Huo[a,b], Xin Ran[a,b], Guanben Du[a,b,*], Long Yang[a,b,*]

[a] Yunnan Provincial Key Laboratory of Wood and Bamboo Biomass Materials，Southwest Forestry University, Kunming, 650224, China

[b] Key Laboratory for Forest Resources Conservation and Utilization in the Southwest Mountains, Ministry of Education, Southwest Forestry University, Kunming 650224, China

[#]These two authors contributed to this work equally

*Corresponding Authors

guanben@swfu.edu.cn (G. Du)

lyang@swfu.edu.cn (L. Yang)

16 **Table S1**. Compositions of the PAM-CAs hydrogels.

Sample	CAs solution (mg)	Chl solution (mg)	H_2O (mg)	MBA (mg)	1173 (mg)	AM (mg)
PAM	0	0	7500	3	30	2500
PAM-Chl	0	3500	4000	3	30	2500
PAM-CAs	3500	0	4000	3	30	2500
PAM-CAs-35%AM	3500	0	3000	3	30	3500

17

18

Table S2. The yields of CAs.

Batch	1	2	3
Yield (%)	46.19	46.65	47.33
Average yield (%)		46.72	

Table S3. Comparison of this work with previous studies.

name	Stress (kPa)	Strain（%）	Water content (%)	Specimen geometry	Test rate (mm min^{-1})	Network structure
This work	1039	2496	65	dumbbell-shaped	100	single network
SAS_4	400	1 984	~76	strip-shaped	200	double network
PAM-ACC	350	1 150	~67.5	strip-shaped	20	single network
CNF/PEDOT:PSS/PAM	230	1 881	~63	strip-shaped	50	double network
PAAm-Cel	201	1 500	~66.7	strip-shaped	10	double network
PLS-n	450	2 060	~75	dumbbell-shaped	100	single network
PAM/CCNF/C-CNTs/PA(MCTP)	50	1 566	/	strip-shaped	50	double network
PDA@CNT/PAM	18	730	~78	strip-shaped	20	single network
PAM/VSNPs/DA@PPy	447	1 340	/	strip-shaped	20	single network
CPAM	1 840	487	~35	strip-shaped	20	double network

Supporting Figures

Figure S1. Photographs of chlorophyll (Chl) and CAs solutions.

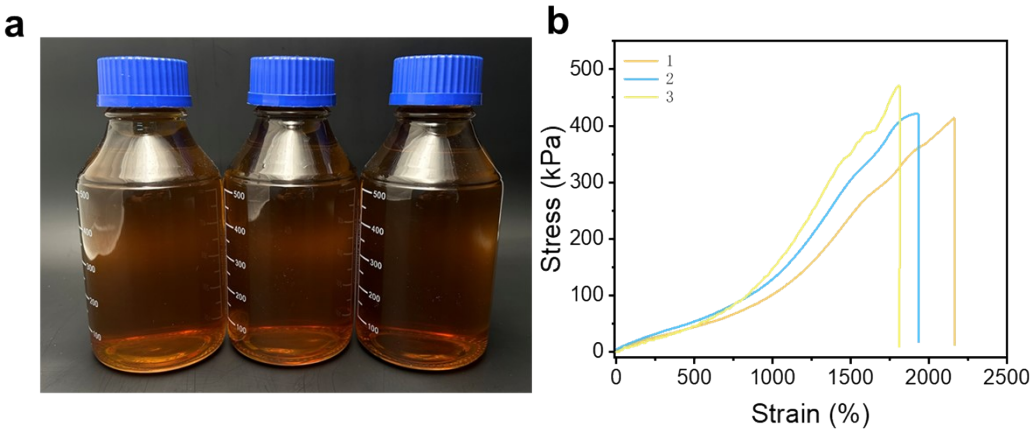

Figure S2. (a) Digital photographs of scalable preparation of CAs. (b) Stress-strain curves of PAM-CAs hydrogels fabricated from three batches of CAs.

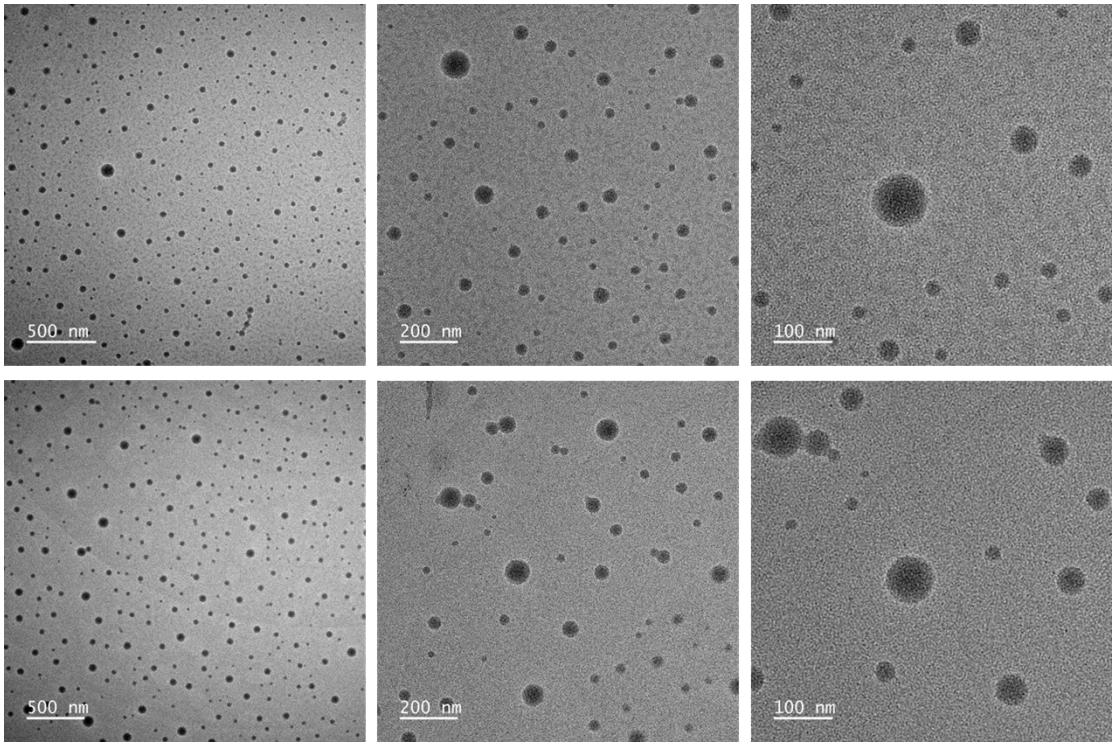

Figure S3. TEM images of CAs.\

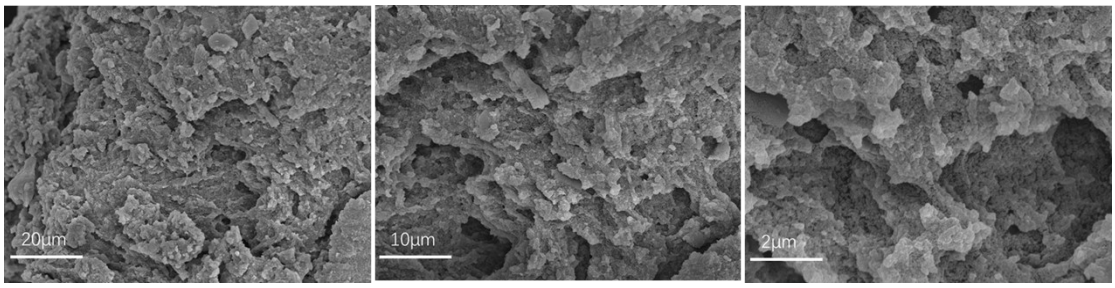

Figure S4. SEM images of CAs.

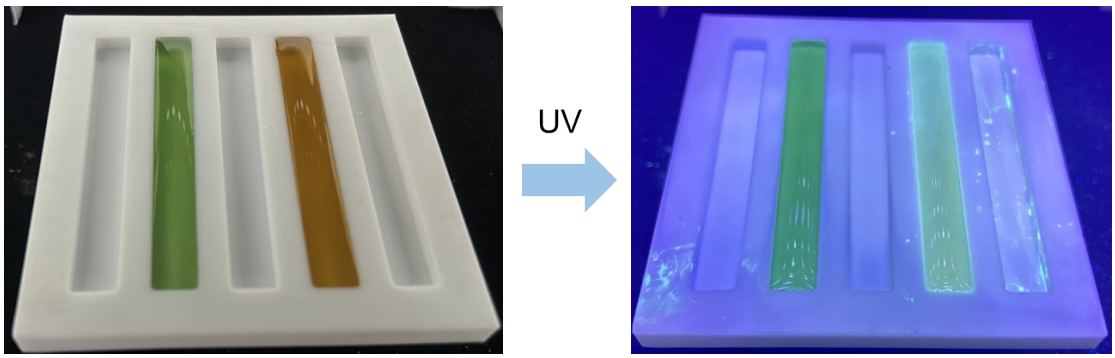

Figure S5. Digital photographs of CAs under UV excitation.

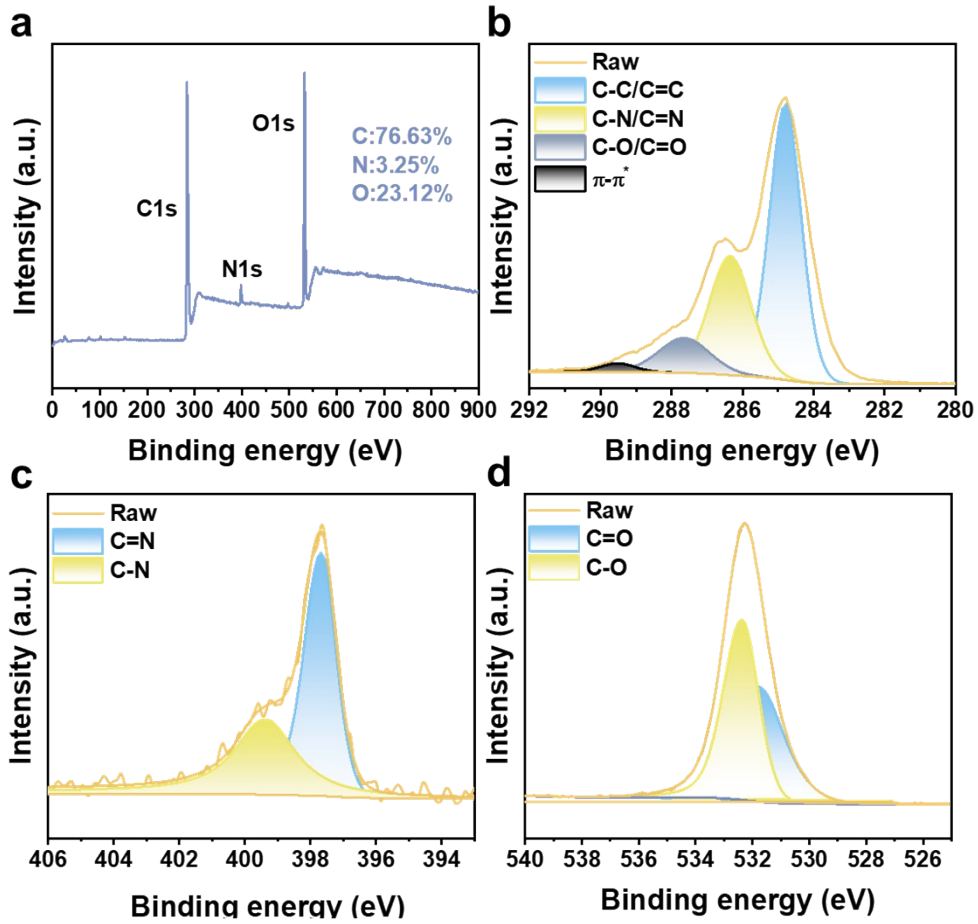

Figure S6. (a) The XPS overall spectrum of CAs. (b) The XPS spectrum of CAs scanned at C 1s. (c) The XPS spectrum of CAs scanned at N 1s. (d) The XPS spectrum of CAs scanned at O 1s.

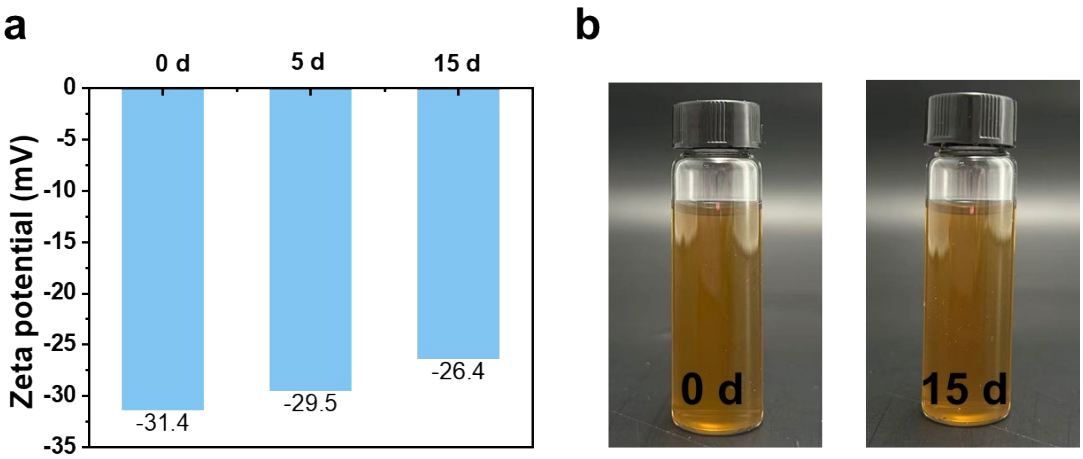

44

45 Figure S7. (a) Zeta potentials of CAs measured at different storage times. (b) Digital

46 photographs of CAs dispersions at day 0 and after 15 days of storage.

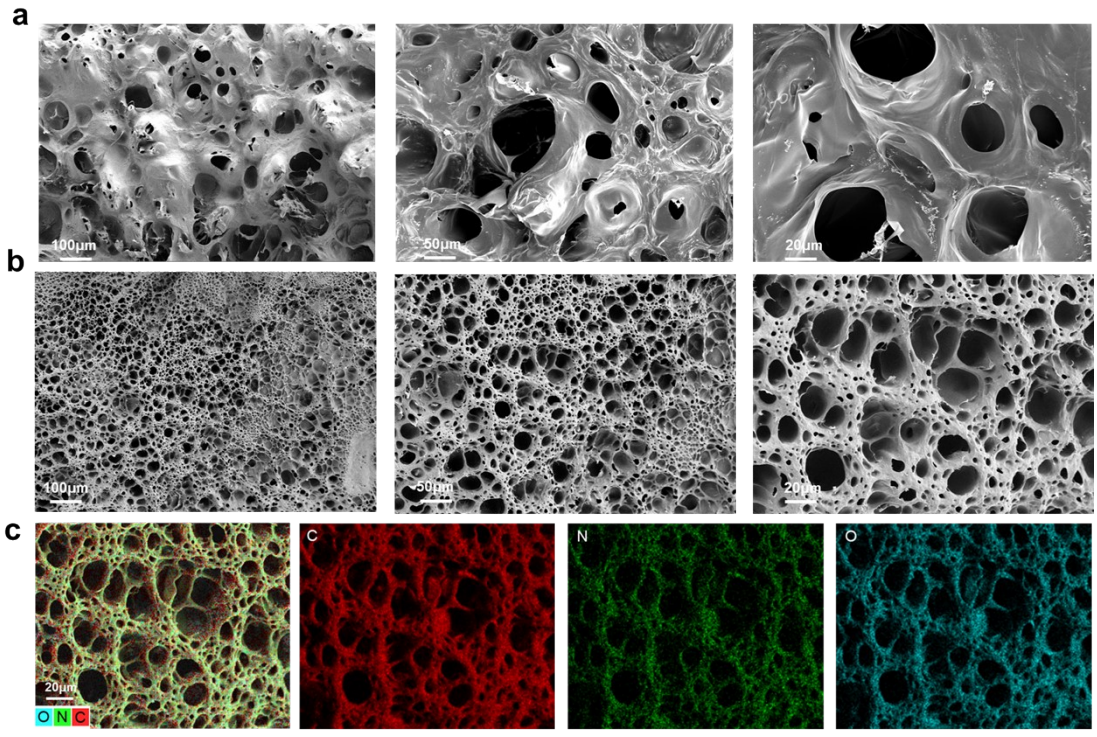

47

48 Figure S8. The SEM image of (a) PAM and (b) PAM-CAs hydrogels. (c) Scanning

49 electron microscopy and EDS of cross section of the PAM-CAs hydrogel.

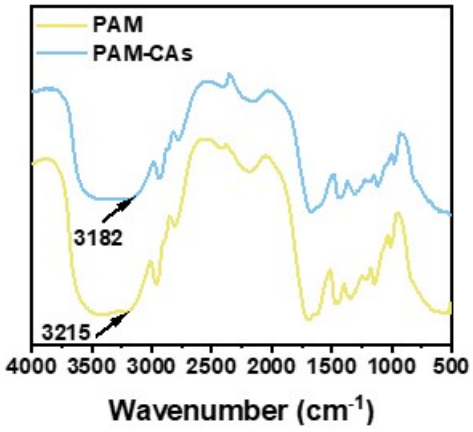

50

51 Figure S9. Fourier transform infrared (FT-IR) spectra of PAM and PAM-CAs

52 hydrogels.

53

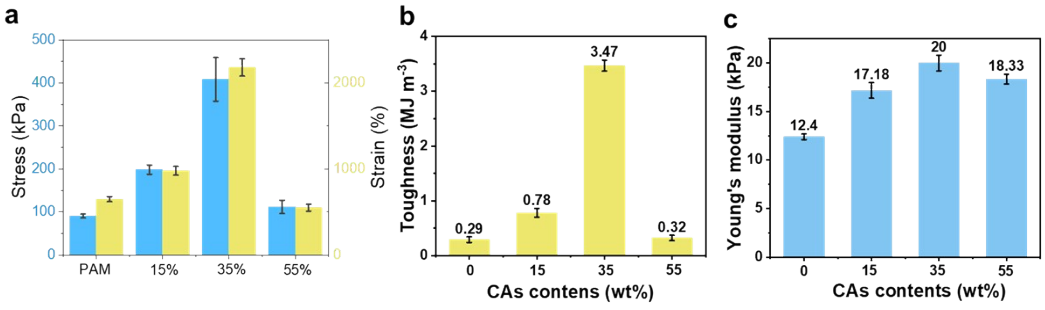

54

55 Figure S10. (a) Tensile strength and elongation at break, (b) toughness, and (c)

56 Young's modulus of PAM–CAs hydrogels with varying CAs contents.

57

58

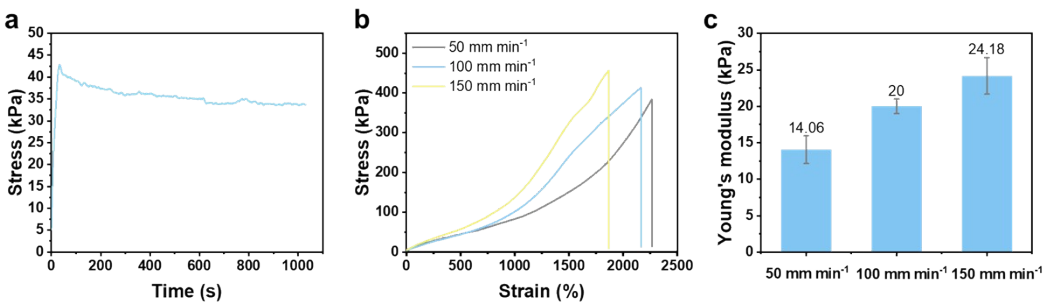

59

Figure S11. (a) Stress-relaxation curves of the PAM-CAs hydrogel. (b) Stress–strain curves of the PAM-CAs hydrogel at different stretching rates. (c) Corresponding Young's modulus.

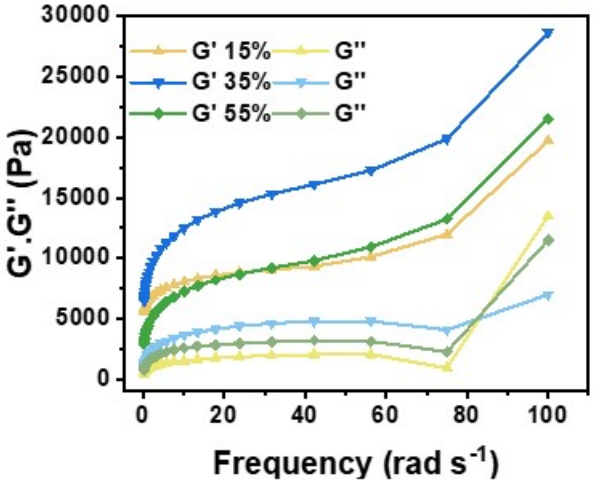

Figure S12. Rheological behaviors of PAM-CAs hydrogels with different CAs contents as a function of angular frequency.

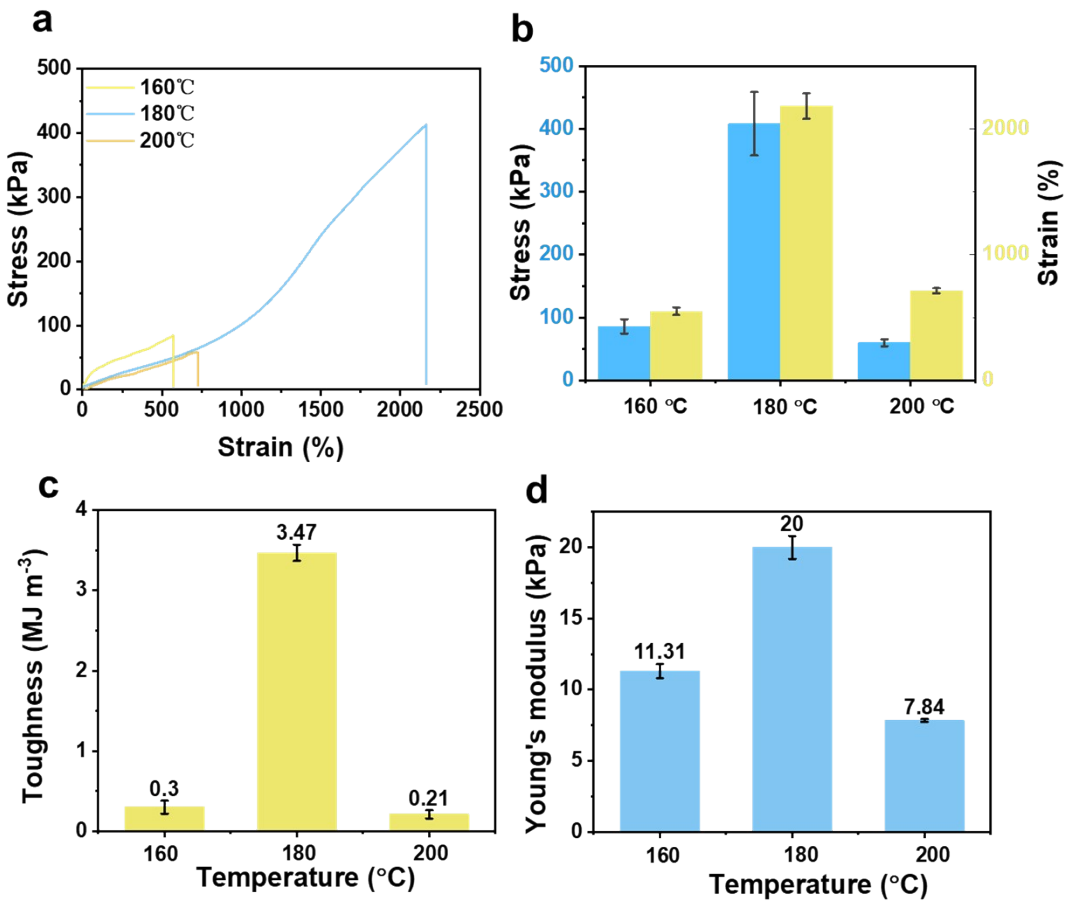

66

67 Figure S13. (a) Stress–strain curves, (b) Tensile strength and elongation at break, (c)

68 toughness, and (d) Young's modulus of PAM–CAs hydrogels carbonized at different

69 temperatures.

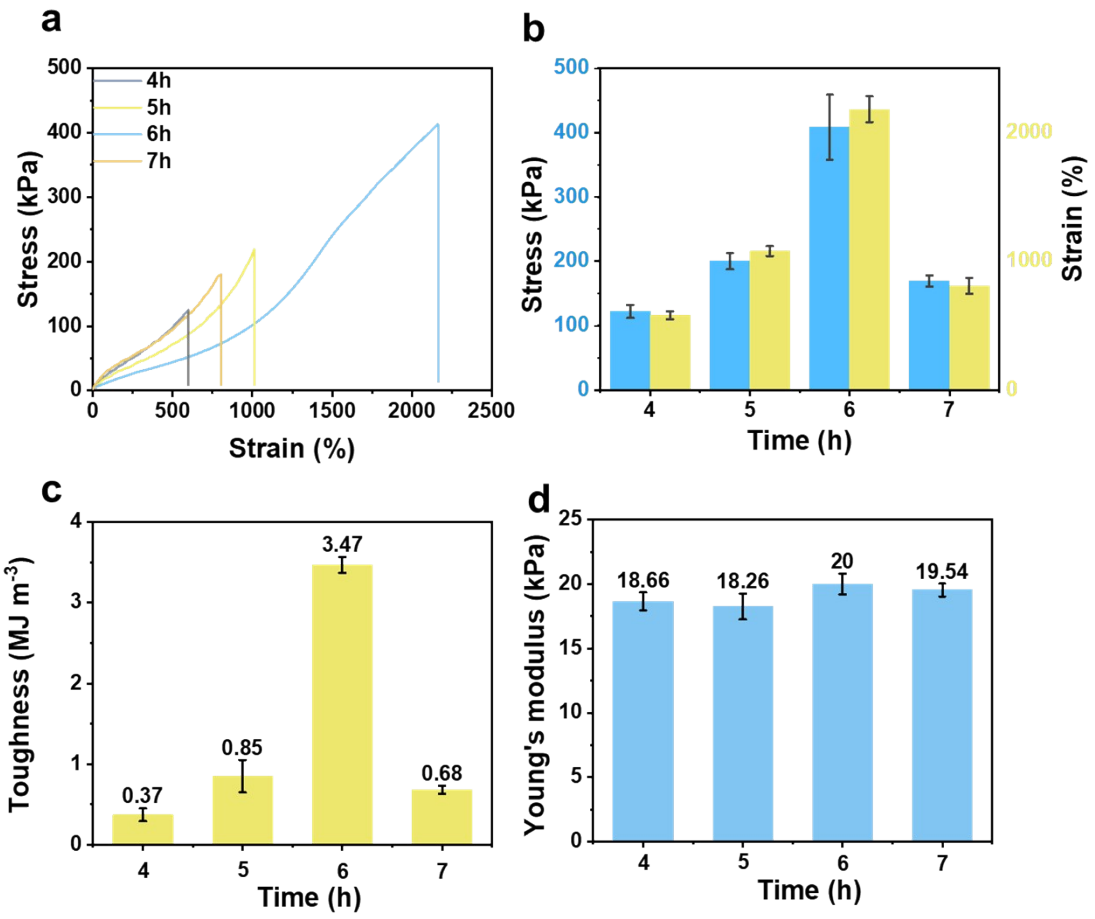

70

71 Figure S14 (a) Stress-strain curves, (b) Tensile strength and elongation at break, (c)
72 Toughness and (d) Young's modulus of PAM-CAs hydrogels with varying
73 carbonization times.

74

75

76

77

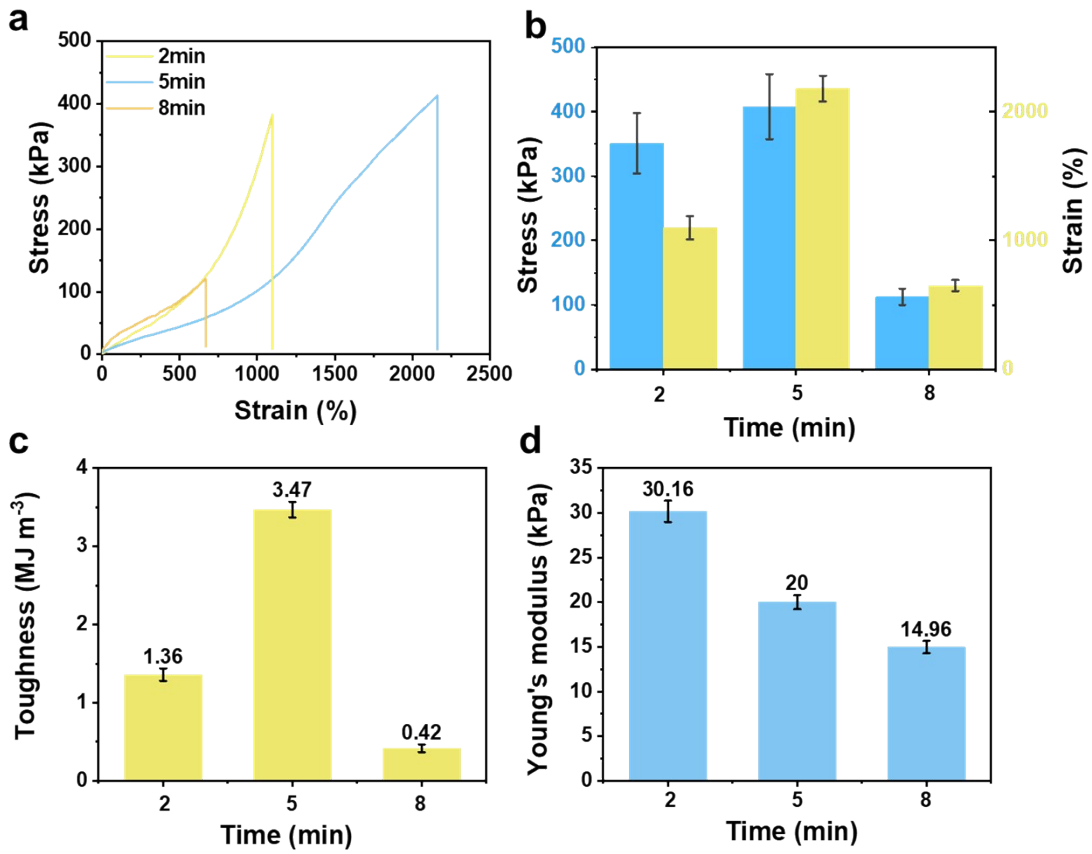

78

79 Figure S15 (a) Stress-strain curves, (b) Tensile strength and elongation at break, (c)

80 Toughness and (d) Young's modulus of PAM-CAs hydrogels with varying light-

81 curing time.

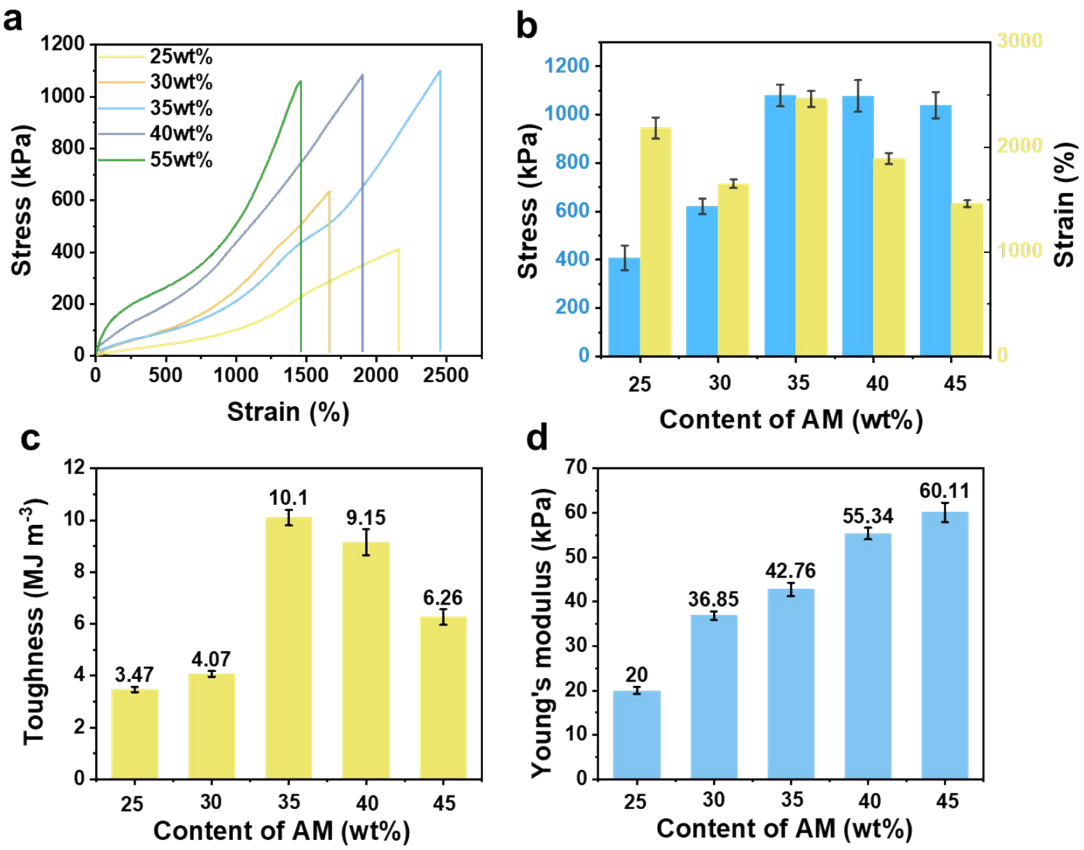

82

83 Figure S16. (a) Stress-strain curves, (b) Tensile strength and elongation at break, (c)

84 Toughness and (d) Young's modulus of PAM-CAs hydrogels with varying AM

85 concentrations.

86

87

88

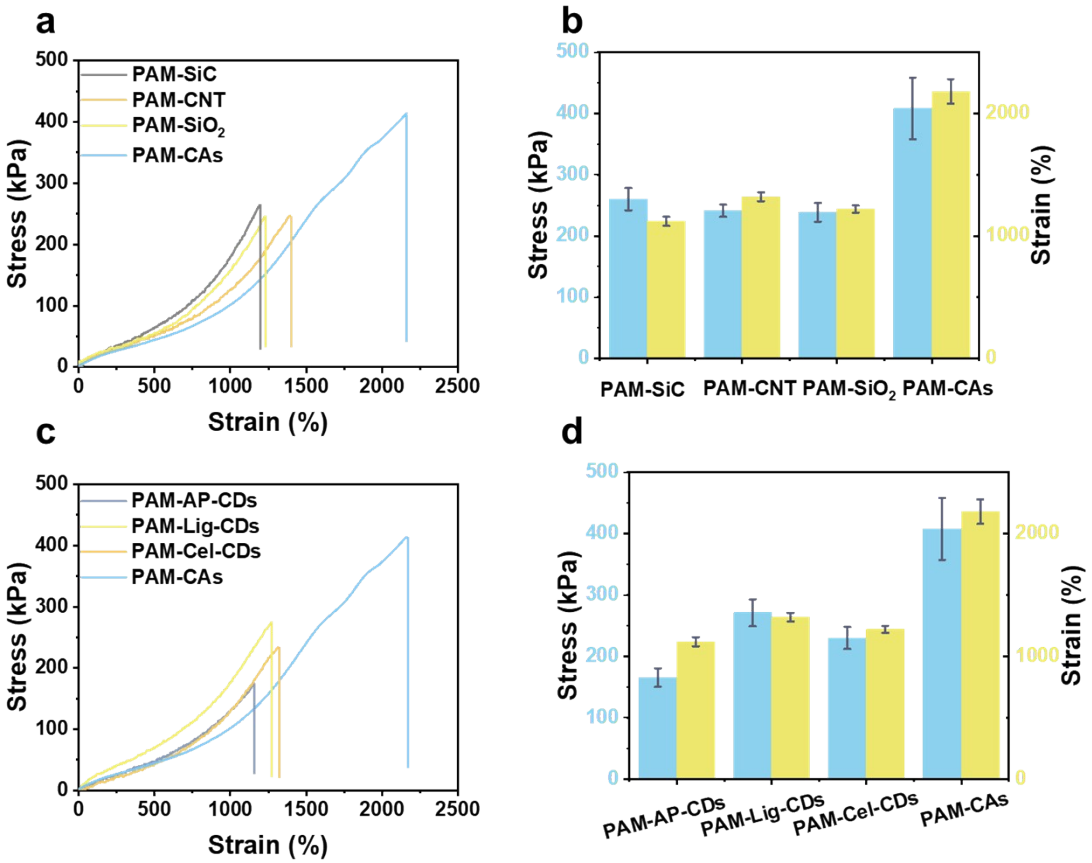

89

90 Figure S17. (a) Stress–strain curves and (b) Tensile strength and elongation at break
91 of PAM–CAs, PAM–CNT, PAM–SiO_2, and PAM–SiC hydrogels. (c) Stress–strain
92 curves and (d) Tensile strength and elongation at break of PAM–CAs, PAM–AP-CDs,
93 PAM–Lig-CDs, and PAM–Cel-CDs hydrogels.

94

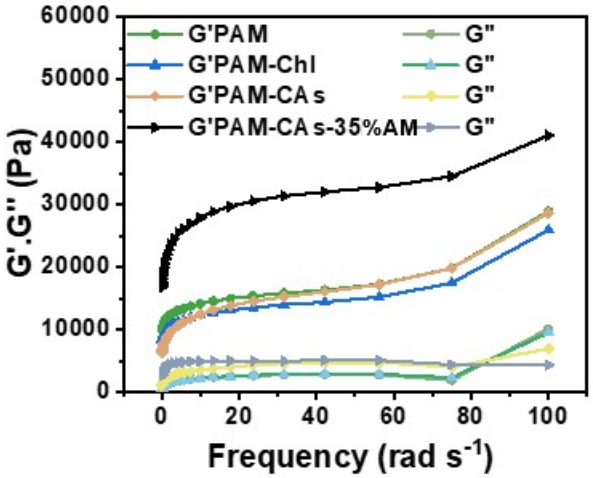

95

96 Figure S18. Rheological behaviors of PAM, PAM-Chl, PAM-CAs, and PAM-CAs-

97 AM35% hydrogels as a function of angular frequency.

98

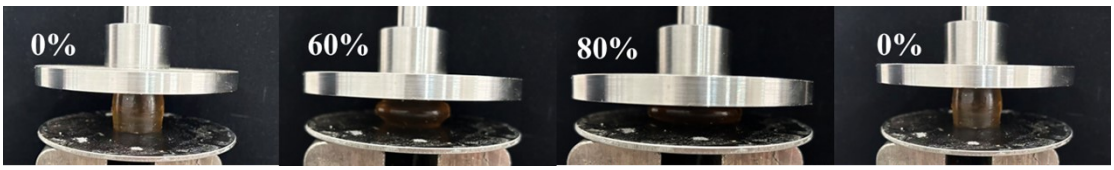

99

100 Figure S19. Schematic diagram of compressive deformation of PAM-CAs hydrogels.

101

102

103

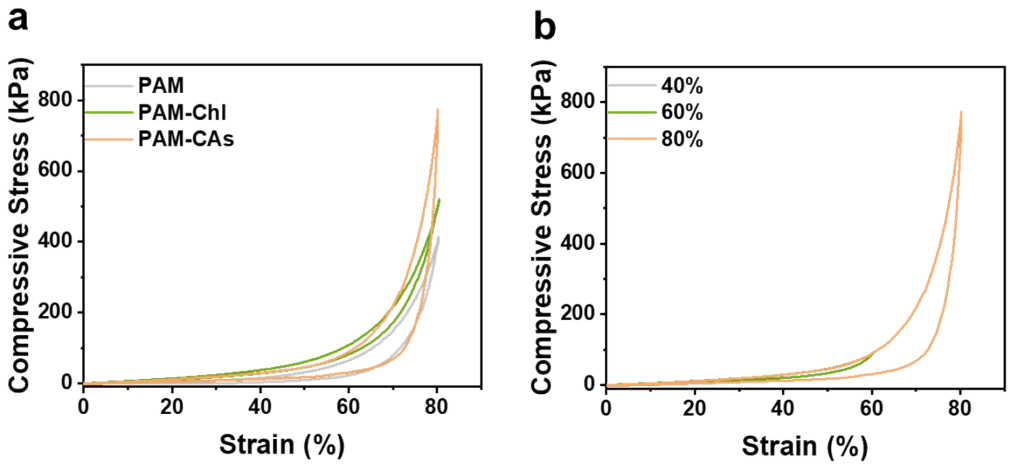

104

105 Figure S20. (a) Compression performances of PAM, PAM-Chl and PAM-CAs
106 hydrogels. (b) Compression performances of PAM-CAs hydrogels under different
107 strains.

108

109

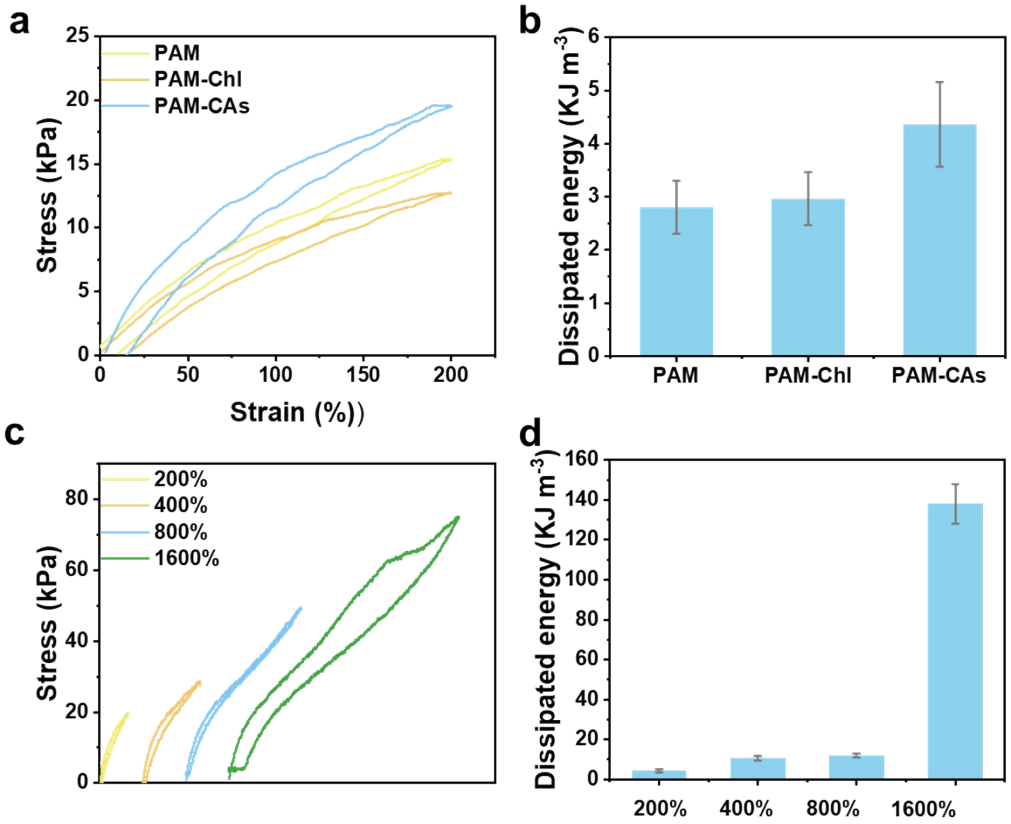

110

111 Figure S21. (a) Loading–unloading tensile curves of PAM, PAM-Chl, and PAM-CAs
112 hydrogels at 80% strain, and (b) the corresponding energy dissipation. (c) Loading-
113 unloading tensile tests of PAM-CAs hydrogels at 200%, 400%, 800%, and 1600%
114 strain, and (d) the corresponding energy dissipation.

115

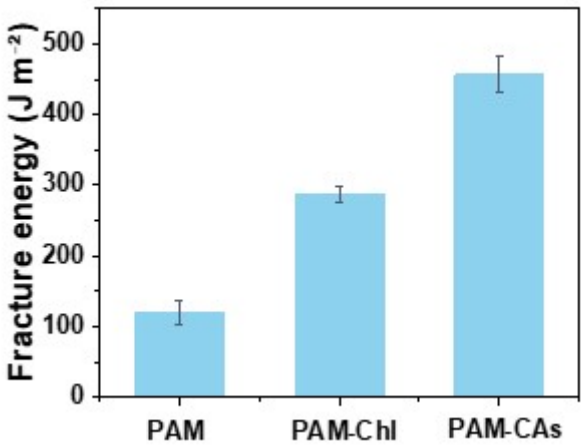

116

117 Figure S22. Fracture energy of PAM, PAM-Chl, and PAM-CAs hydrogels.

118

119

120

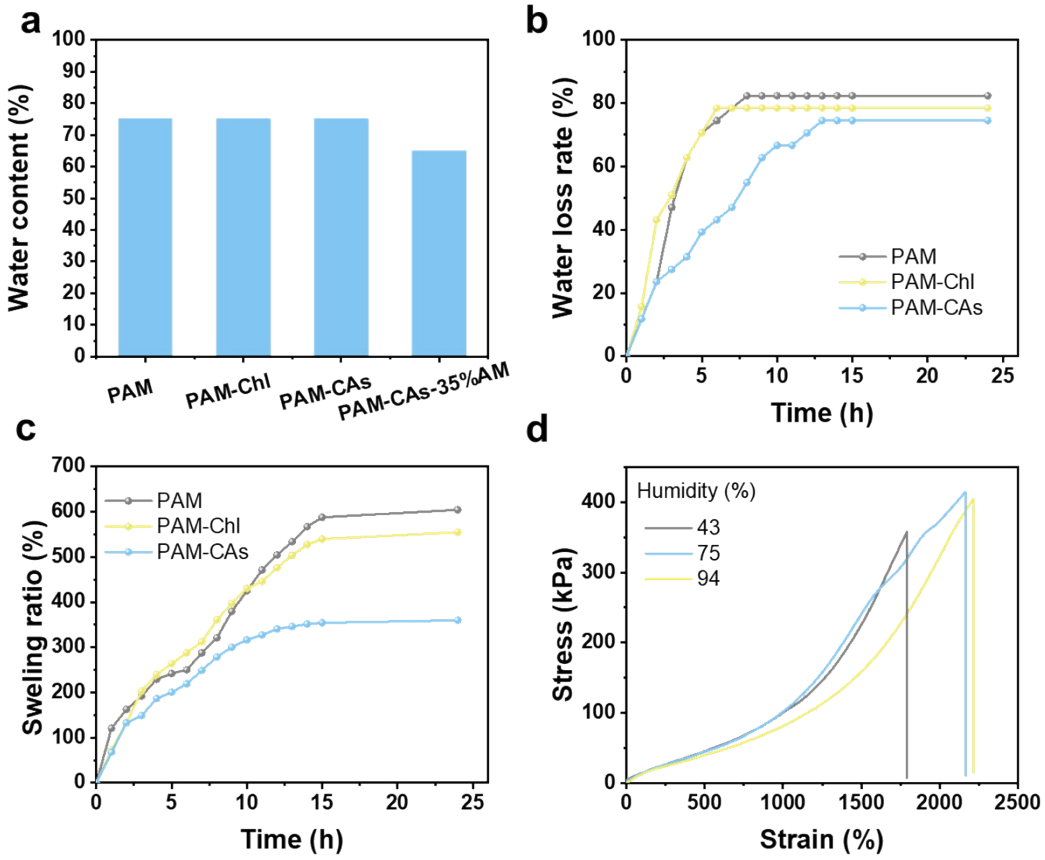

121

122 Figure S23. (a) Equilibrium water content of PAM, PAM-Chl, PAM-CAs, and PAM-
123 CAs-35% AM hydrogels. (b) Water loss ratio of PAM, PAM-Chl, and PAM-CAs
124 hydrogels at room temperature. (c) Swelling ratio of PAM, PAM-Chl, and PAM-CAs
125 hydrogels in water. (d) Tensile stress–strain behavior of the PAM-CAs hydrogel
126 under different humidity conditions.

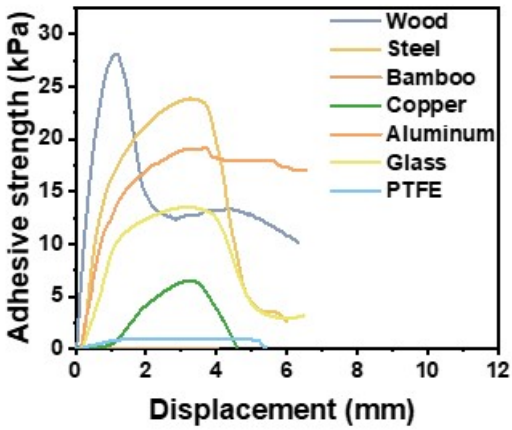

127

128 Figure S24. Adhesion strength-displacement curves of PAM-Chl hydrogels using

129 different substrates.

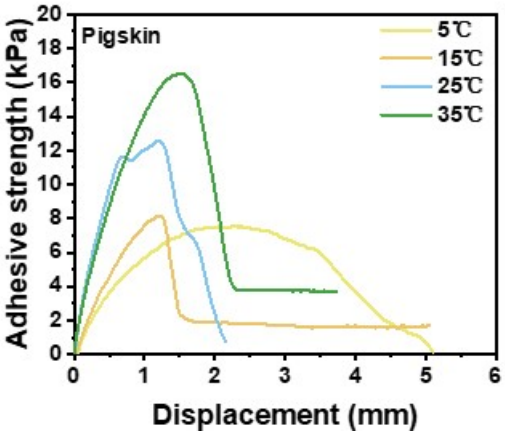

130

131 Figure S25. Adhesion strength versus displacement curves for PAM-CAs hydrogels at

132 different temperatures.

133

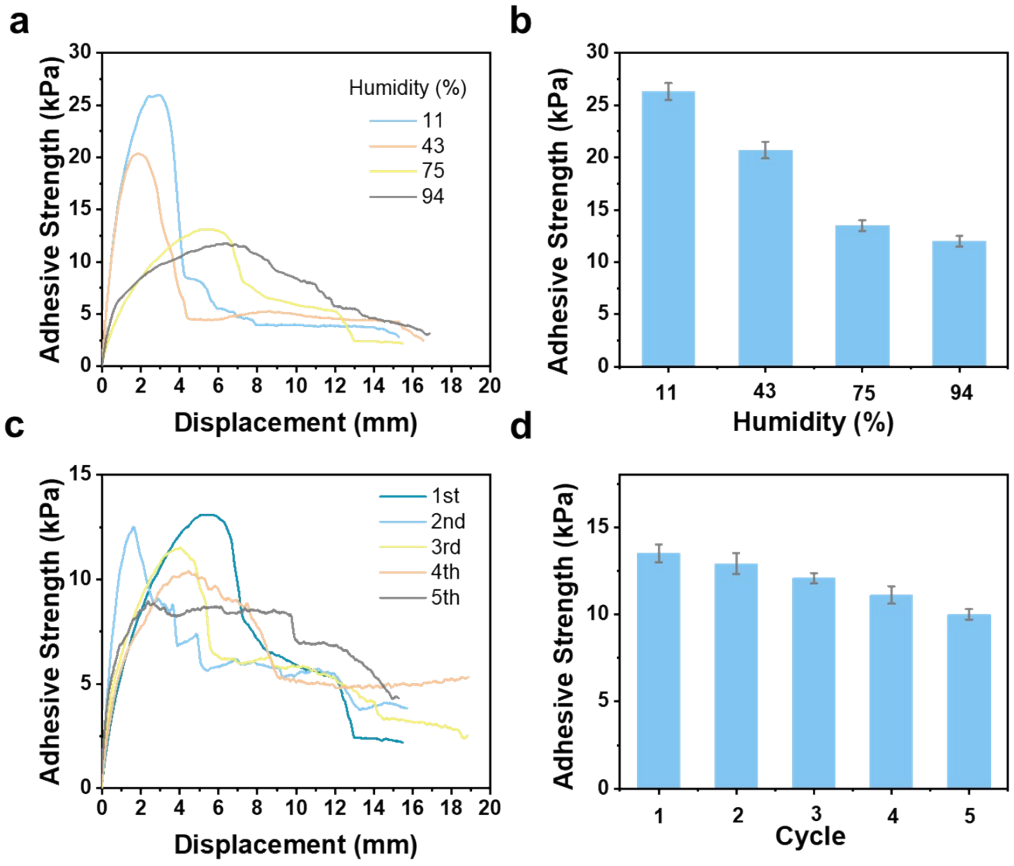

134

135 Figure S26. (a) Adhesion force–displacement curves of the PAM-CAs hydrogel on

136 porcine skin under different humidity conditions. (b) Corresponding adhesion strength.

137 (c) Cyclic adhesion force–displacement curves of the PAM-CAs hydrogel on porcine

138 skin during repeated adhesion tests. (d) Corresponding adhesion strength.

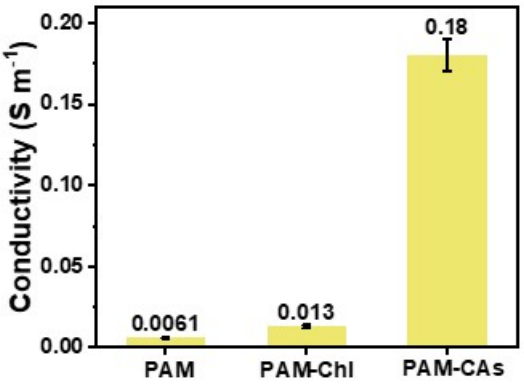

139

140 Figure S27. Conductivities of PAM, PAM-Chl and PAM-CAs hydrogels.

141

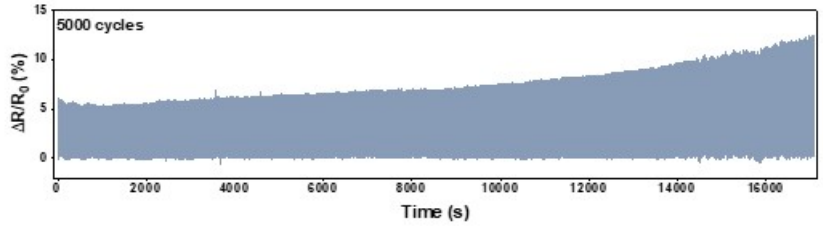

142

143 Figure S28. Real-time resistance changes of PAM-CAs hydrogels subjected to 5000

144 cycles at 10% strain.

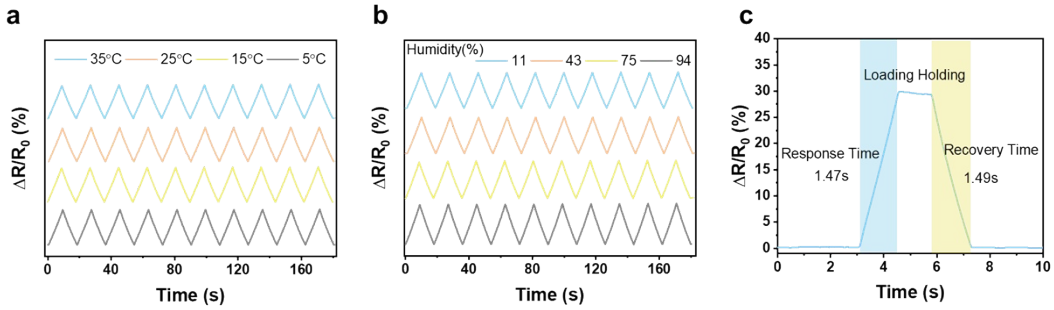

145

146 Figure S29. (a) Resistance variation of the PAM-CAs hydrogel at different

147 temperatures. (b) Resistance variation of the PAM-CAs hydrogel under different

148 humidity conditions. (c) Response and recovery times of the PAM-CAs hydrogel

149 sensor.

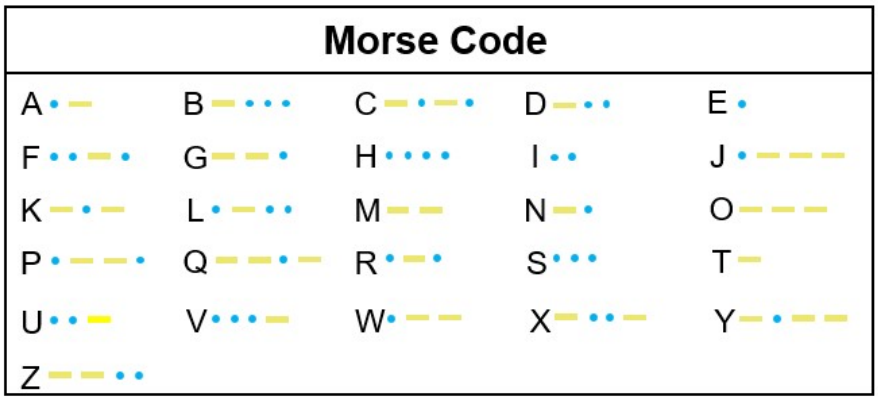

150

151 Figure S30. Morse code symbols representing the letters used for encoding.

Video S1. Tear-resistance demonstration of PAM hydrogel.

Video S2. Tear-resistance demonstration of PAM-CAs hydrogel.